

Temporal evolution of an ultrathin, noncrystalline ice deposit at crystallization near 160 K studied by FT-IR reflection–absorption spectroscopy¹

S. Mitlin and K.T. Leung

Abstract: The temporal evolution of the OH stretching modes of a noncrystalline ice deposit upon annealing followed by crystallization near 160 K has been investigated by FT-IR reflection–absorption spectroscopy. Using the earlier theoretical results from Whalley (E. Whalley. *Can. J. Chem.* **55**, 3429 (1977)) and from Buch and Devlin (V. Buch and J.P. Devlin. *J. Chem. Phys.* **110**, 3437 (1999)), the most prominent changes in these modes have been characterized for the first time. A dynamical picture of the structural transformation during crystallization has been developed, and it supports the observation that crystallization proceeds directly from a noncrystalline to a crystalline state without any long-lived intermediate state structurally different from its noncrystalline predecessor.

Key words: crystallization, noncrystalline ice, FT-IR reflection–absorption spectroscopy, temporary evolution.

Résumé : Faisant appel à la spectroscopie de réflexion–absorption infrarouge à transformée de Fourier, on a étudié l'évolution en fonction du temps des modes d'élongation OH d'un dépôt de glace non cristalline soumise à un réchauffement puis à une cristallisation près de 160 K. Utilisant des résultats théoriques antérieurs de Whalley (E. Whalley. *Can. J. Chem.* **55**, 3429 (1977)) et d'autres de Buch et Devlin (V. Buch et J.P. Devlin. *J. Chem. Phys.* **110**, 3437 (1999)), on a pu caractériser les changements les plus importants dans ces modes pour la première fois. On a développé une image dynamique de la transformation de structure au cours de la cristallisation et elle est en accord avec l'observation que la cristallisation procède directement d'un état non cristallin à un état cristallin sans l'intermédiaire d'un état de longue durée qui serait différent d'un point de vue structural de son prédécesseur non cristallin.

Mots clés : cristallisation, glace non cristalline, spectroscopie de réflexion–absorption infrarouge à transformée de Fourier, évolution en fonction du temps.

[Traduit par la Rédaction]

Introduction

At cryogenic temperature, water medium exhibits both crystalline form, such as cubic Ic and hexagonal Ih arrangements, and noncrystalline (nc) form. For the nc-ice form, a number of distinct polyamorphs can be generally classified according to their density: the high-density amorph (HDA) with density $\rho > 1.1 \text{ g cm}^{-3}$ and the low-density amorph (LDA) with $\rho \sim 0.94 \text{ g cm}^{-3}$ (1–4). Physico-chemical properties of these two types of polyamorphs are known to be quite different, which suggests qualitative differences in the packing arrangements in their intrinsic local structures and in the arrangements of the network of hydrogen bonds (5). Using elastic neutron diffraction, Finney et al. (5) found structural similarities between the LDA and hexagonal ice and between HDA and liquid water. Furthermore, the observable bulk and surface properties of a particular nc-ice sample ap-

pear to depend critically on the preparation method and the post-growth history, as expected for the metastable states that are structurally unrelaxed. In particular, the inelastic neutron scattering measurements by Kolesnikov et al. (6) confirmed the dependence of the local structure of the LDA ice on the preparation method. Computer simulations (7–10) revealed that the LDA could exhibit a fractal structure with a large variation in the local density. However, the characteristic size of the intrinsic “building block” (or molecular cluster) of the fractal structure remains unknown.

The morphology of the nc-ice medium has also been found to depend on the preparation technique. In particular, by varying the direction of the incident (water) molecular beam, Stevenson et al. (11) observed a systematic change in the morphology of the vapour-deposited LDA ice films, which could accommodate nitrogen as much as $2700 \text{ m}^2 \text{ g}^{-1}$ at 22 K and $640 \text{ m}^2 \text{ g}^{-1}$ at 77 K, if prepared at glancing incidence. Large uptakes of argon and methane by the LDA ice films have also been reported recently by Dohlanek et al. (12), which similarly suggests the presence of a fractal, grassy-like structure for the low-temperature vapour-deposit, in agreement with the earlier studies of Mayer and Pletzer (13) and Laufer et al. (14) that support a morphologically porous medium for the LDA. As expected for fractal behaviour, the LDA appears to exhibit recurrent features on different length scales, from $\sim 10 \text{ \AA}$ for a typical cluster size in the

Received 8 February 2004. Published on the NRC Research Press Web site at <http://canjchem.nrc.ca> on 31 August 2004.

S. Mitlin and K.T. Leung,² Department of Chemistry, University of Waterloo, Waterloo, ON N2L 3G1, Canada.

¹This article is part of a Special Issue dedicated to the memory of Professor Gerhard Herzberg.

²Corresponding author (e-mail: tong@uwaterloo.ca).

hydrogen-bonding network (8) to larger though yet-to-be-determined nanopores (13, 15), and to much larger mesoscopic features (14).

Crystallization of a LDA medium has been found to occur abruptly at a rapid rate over a narrow temperature range above 150 K (16). At a lower temperature, crystallization is too slow to be observed at a laboratory timescale, in spite of the metastable nature of nc ice with respect to its crystalline polymorphs. However, internal motions in these nc-ice structures have clearly been discernible below 130 K. In particular, on annealing thick LDA ice films vapour-deposited at 77 K, Hallbrucker et al. (17) observed a rapid reduction in the surface area from several hundreds to 40 m² g⁻¹ at 113 K, which was interpreted as the result of the collapse of micropores accompanied by significant exothermic effects. By hyperquenching the micrometer-sized water droplets at 140 K, Kohl et al. (16) were able to obtain LDA samples that exhibit no exothermic effects upon a small anneal, which leads us to suggest that just above the expected glass-to-liquid transition temperature, the hyperquenched nc-ice samples become substantially more homogeneous though remain primarily noncrystalline. By measuring the time dependence of the OH dangling-bond signal of vapour-deposited nc-ice films by FT-IR reflection-absorption spectroscopy (FT-IR-RAS), Zondlo et al. (18) showed that the collapse of the micropores occurs rapidly on a timescale of 10³–10⁴ s at a temperature as low as 105 K, indicative of plausible structural relaxation. By measuring the isotope intermixing, Smith and Kay (19) and Smith et al. (20) found the self-diffusion coefficient ($1 \times 10^{-16} - 1 \times 10^{-13}$ cm² s⁻¹) in the temperature range of 146–155 K for nc-ice films to be substantially larger than that of crystalline films. Furthermore, they also determined the apparent Arrhenius activation energy for diffusion in a crystalline film to be 14 kcal mol⁻¹ and that in an amorphous film to be as high as 41 kcal mol⁻¹. These observations led them to favour the existence of supercooled liquid domains in the temperature range of 145–155 K, which lies between the onset of plausible glass-to-liquid transition in the LDA (135 K) (17) and the onset of crystallization (160 K). Thermal desorption studies by Dohnalek et al. (21, 22) revealed the difference in the desorption spectra of N₂ from the surfaces of nc- and crystalline-ice films and the dependence of the desorption spectra on the annealing history of the pore-less nc-ice films, both of which have been used to follow the crystallization kinetics. The crystallization of thin (15–150 bilayers) nc-ice films deposited on Pt (111) and on smooth crystalline ice films was found to be consistent with bulk nucleation and three-dimensional growth of the crystalline phase, except for very thin amorphous deposits on the crystalline-ice film that was found to crystallize by a two-dimensional substrate-induced growth mechanism. These studies appear to be in accord with the direct transformation of solid amorphous to ice crystallites without the formation of an intermediate liquid-like amorphous state (22). In an earlier calorimetric work, MacFarlane and Angell (23) argued that the glass-to-liquid transition in nc ice should be above the crystallization onset at 160 K, because given the very large nucleation rate for water, the driving force towards crystallization (being proportional to the difference between the homogeneous nucleation temperature and the glass-to-liquid transition

temperature) should be sufficiently large. In more recent studies, Velikov et al. (24) further argued that the glass-to-liquid transition should be above the onset of crystallization and have estimated the former transition temperature to be 165 K.

To date, there has been no direct spectral evidence for the presence of the glass-to-liquid transition before the onset of crystallization, although it is possible that no spectral difference in the OH stretching modes exist between the glass amorphous and liquid-like amorphous states. The present work examines the spectral evolution of the relevant OH stretching modes before and during crystallization of an nc-ice film by using FT-IR-RAS, with the goal to not only assign these spectral features with the vibrational modes in nc and polycrystalline (pc) ice films, but also correlate the spectral changes to the structural evolution.

Experimental details

The details of the experimental setup and procedures have been described elsewhere (25). Briefly, the FT-IR-RAS experiments were conducted in an ultrahigh vacuum (UHV) chamber evacuated to a base pressure better than 3×10^{-9} torr (1 torr = 133.322 4 Pa). Ice films were grown by water vapour deposition on an optically flat polycrystalline copper disk mounted on a four-motion manipulator. The copper substrate could be cooled to 120 K or annealed to a preset temperature (up to 400 K) by a resistance heater attached to the backside of the substrate. The substrate temperature was monitored by two K-type thermocouples separately fastened to the front surface of the copper disk, with the accuracy of the temperature measurement of ± 1 K. Deposition of the ice films was performed by backfilling of the UHV chamber with vapours of H₂O (Millipore) or of D₂O (Isotech) with a small fraction of HDO by a variable leak valve. The liquid water samples were thoroughly degassed by several freeze-pump-thaw cycles prior to use. The deposition pressure was measured by an uncalibrated ionization gauge and held at 1×10^{-6} torr (1 torr = 133.322 4 Pa) unless stated otherwise.

The IR beam from a FT-IR spectrometer (Bruker Equinox 55) was directed to the target surface at $\sim 83^\circ$ from the surface normal by two external mirrors. The specularly reflected light was collected by another external focusing mirror positioned on the opposite side of chamber, and focused onto a mercury-cadmium-telluride detector. The entire optical path was purged with dry N₂ gas. Spectral data are represented in units of absorbance defined as $A = -\log(R/R_0)$, where R/R_0 is the ratio of reflectances with and without the ice film. In an attempt to elucidate the nature of the observed spectral changes with increasing film thickness, the Fresnel method applied to a triple-layer (vacuum-ice-metal) stratified medium (18, 26, 27) was used to simulate the FT-IR-RAS spectra using optical constants for pc and nc ice available in the literature (28, 29). Details of our computational procedure have been given in our earlier work (25).

Results and discussion

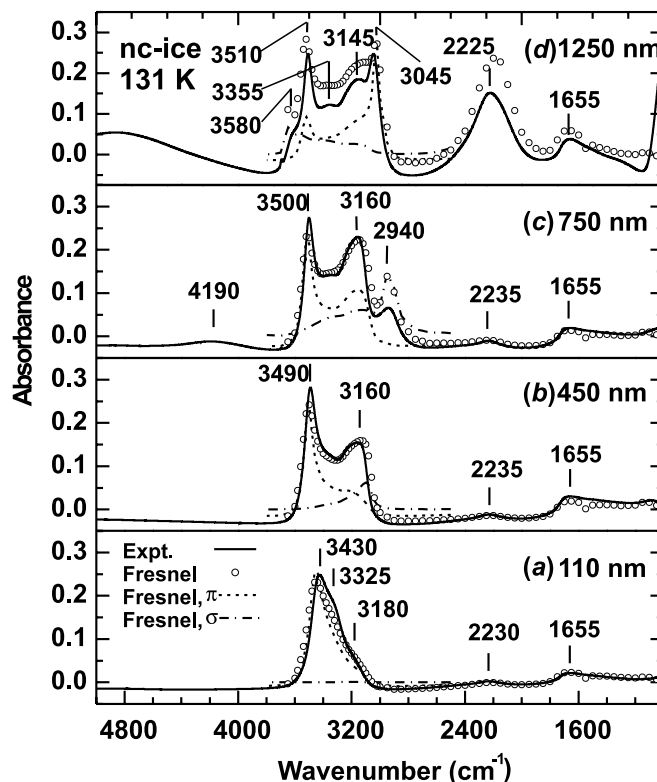
The growth of pc- and nc-ice films by vapour deposition has been studied by FT-IR-RAS over a range of film thick-

ness from 10 to 1500 nm. In accord with earlier results (18, 25, 30), there are two established optical effects associated with the reflection-absorption of IR light in a stratified ice medium: (i) blue shift and profile deformation of the OH stretch (the strongest RA band in the ice spectrum) with respect to that obtained in the transmission mode, and (ii) optical interference in the smooth films. There is generally good agreement between the experimental spectra and the simulated Fresnel spectra of ice films for a wide range of thickness from 50 to 1500 nm. However, there are other possible spectral effects associated with the particle size and shape of the ice medium and with scattering from a rough film-vacuum interface, which are more difficult to characterize. These effects could become dominant in the present cases of interest, i.e., the early stage of deposition and during annealing and crystallization. The spectral effects associated with the size and shape of the constituent particles in the absorbing medium were investigated theoretically for finite-sized ionic crystals by Englman and Ruppin (31) and experimentally demonstrated for KCl films and crystals by Martin (32). Later, Buch and Devlin (33) provided a spectral simulation of the crystalline ice in the forms of a sphere and a slab, and illustrated that the OH stretching band strongly depends on not only the polarization of the light but also the shape of the absorbing medium. Following the theoretical treatment of Buch and Devlin (33) and the earlier spectral assignment of the OH stretch features by Whalley (34), we provide a detailed interpretation of the experimentally observed RA features of the OH band at the early stage of pc-ice formation and during crystallization of an ultrathin nc-ice deposit.

FT-IR-RA spectral features of the noncrystalline and polycrystalline ice in the Fresnel regime (for over 50 nm thick films)

Figure 1 shows typical spectra of nc-ice films obtained by water vapour deposition at 1×10^{-6} torr (1 torr = 133.322 4 Pa) with the copper substrate held at 131 K as a function of film thickness. The features near 1655 and 2230 cm^{-1} (Fig. 1a) can be assigned as the OH bending band (ν_2) with contribution from the first overtone ($2\nu_R$) of the hindered rotational lattice mode (ν_R), and as the combination band ($\nu_2 + \nu_R$) of the OH bending and hindered rotation modes, respectively, (35, 36, 37). These features remain essentially in the same peak positions with increasing film thickness. Furthermore, three relatively "stationary" (ν_1, ν_3) OH stretch features at 3490–3510 cm^{-1} (band maximum), 3355 cm^{-1} , and 3160–3145 cm^{-1} can be resolved for film thickness greater than 450 nm (Figs. 1b–1d). For film thickness below 250 nm, the shape of the (ν_1, ν_3) OH stretching band is predominantly determined by reflection-absorption of the π -polarized component of the incident light (Fig. 1a), with negligible contribution from the σ -polarized component. For film thickness greater than 250 nm, the σ -polarized component is generally found to strengthen with the emergence of an interference feature traveling from 3160 cm^{-1} at 450 nm (Fig. 1b) to 2940 cm^{-1} at 750 nm (Fig. 1c) and to 2225 cm^{-1} at 1250 nm (Fig. 1d). Another σ -polarized interference feature near 4190 cm^{-1} for film thickness of 750 nm (Fig. 1c) is also seen to travel to 3580 cm^{-1} for the 1250 nm thick film (Fig. 1d). It is evident that the π -polarized compo-

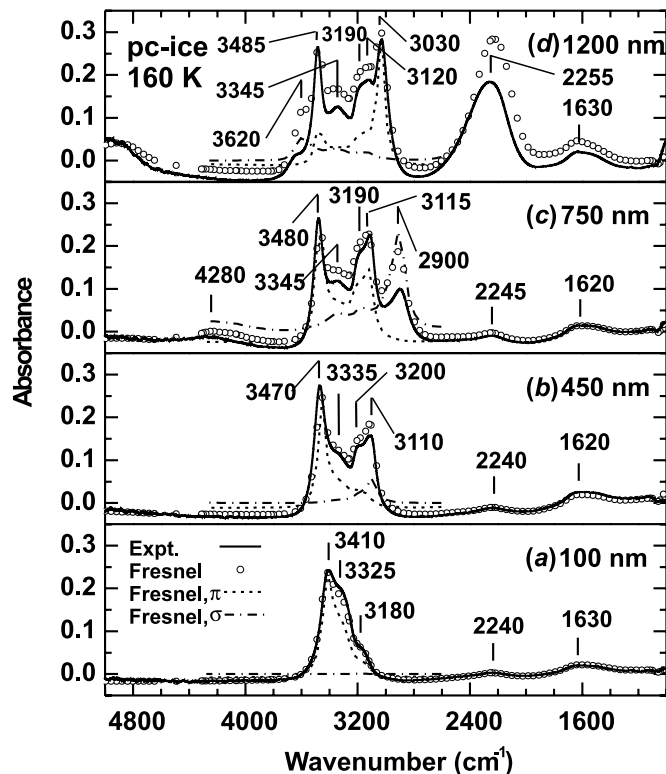
Fig. 1. Comparison of experimental FT-IR-RA spectra of noncrystalline (nc) ice films obtained by vapour deposition at 131 K for (a) 3.5 min, (b) 20.5 min, (c) 33.5 min at 1×10^{-6} torr, and (d) 11 min at 5×10^{-6} torr (1 torr = 133.322 4 Pa) with the corresponding Fresnel spectra for non-polarized light and their σ - and π -polarized components (arbitrarily normalized) involving 110, 450, 750, and 1250 nm thick films, respectively.



nent also contributes prominently to the three aforementioned stationary OH stretch features over the film thickness range covered in Fig. 1. The movement of the main π -polarized feature (near 3430 cm^{-1} for the 110 nm thick film in Fig. 1a) to a higher frequency with increasing film thickness gives rise to the observed blue shift of the band maximum. This shift is therefore related to the physics of reflection-absorption of IR light and not to any possible structural change in the nc-ice network as a result of an increase in the film thickness. For thicker films, the π -polarized interference feature observed at 3160 cm^{-1} for the 750 nm thick film (Fig. 1c) is also found to travel to a lower frequency with increasing film thickness, e.g., 3045 cm^{-1} for the 1250 nm thick film (Fig. 1d).

Figure 2 demonstrates typical spectral evolution of pc-ice films obtained by water vapour deposition at 1×10^{-6} torr (1 torr = 133.322 4 Pa) with the substrate held at 160 K as a function of film thickness. Evidently, three major absorption features related to the vibrational modes of the water molecules in the pc-ice film are also observed: the OH stretching band (ν_1, ν_3) at 3410 cm^{-1} , the first overtone ($2\nu_R$) of the hindered rotational lattice mode ($\nu_R \approx 850 \text{ cm}^{-1}$) (35, 36) at 1630 cm^{-1} with higher-frequency contribution from the OH bending band (ν_2), and the ($\nu_2 + \nu_R$) combination band and (or) the $3\nu_R$ second overtone at 2240 cm^{-1} (Fig. 2a) (36, 37). There is also generally good accord between the experimen-

Fig. 2. Comparison of experimental FT-IR-RA spectra of polycrystalline (pc) ice films obtained by vapour deposition at 160 K and 1×10^{-6} torr (1 torr = 133.322 4 Pa) for (a) 3.5 min, (b) 20 min, (c) 33.5 min, and (d) 52.5 min with the corresponding Fresnel spectra for non-polarized light and their σ - and π -polarized components (arbitrarily normalized) involving 100, 450, 750, and 1200 nm thick films, respectively.



tal spectrum and the corresponding Fresnel spectrum of a pc-ice film for all the film thicknesses depicted in Fig. 2. As with nc-ice films, the residual, non-vibration-related spectral features of the thicker (>100 nm) pc-ice films can be attributed to the σ - and π -polarized IR interference patterns, which are well approximated by the σ - and π -components of the corresponding Fresnel spectra. In particular, the low-frequency shoulder of the σ -polarized profile is seen to travel from 3110 cm^{-1} for the 450 nm thick film (Fig. 2b) to 2900 cm^{-1} for the 750 nm thick film (Fig. 2c), which evidently contributes to the corresponding features at 3110 and 2900 cm^{-1} in the respective experimental spectra. Further increase in the film thickness to 1200 nm causes the σ -polarized feature to move towards the lower frequency, giving rise to the strong enhancement of the spectral intensity at 2255 cm^{-1} (Fig. 2d). Furthermore, a second σ -polarized feature near 4280 cm^{-1} appearing in the spectrum for the 750 nm thick film (Fig. 2c) is also found to migrate to 3620 cm^{-1} for the 1200 nm thick film (Fig. 2d). Similar interference peak movement is also evident for the π -polarized feature at 3115 cm^{-1} for the 750 nm thick film (Fig. 2c), which travels to 3030 cm^{-1} as the film thickness is increased to 1200 nm (Fig. 2d). The evolution of the underlying σ - and π -polarized Fresnel contributions to the overall spectrum of pc ice with increasing film thickness (Fig. 2) is therefore similar to that found for the nc ice (Fig. 1). The observed

movements of the destructive interference peaks generally reflect the quality of film uniformity obtainable for pc ice by vapour deposition.

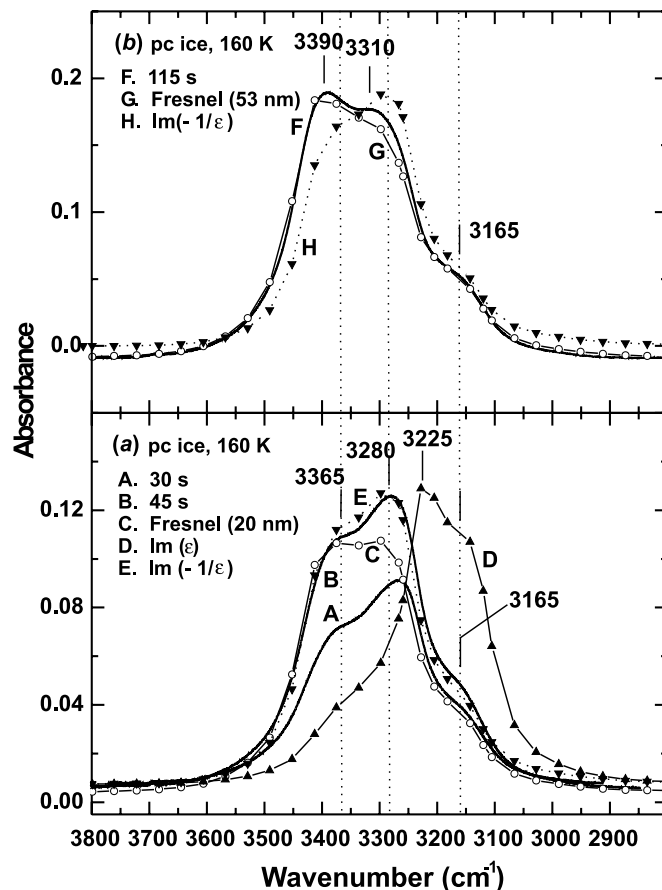
Spectral characterization of the OH (OD) stretch manifold of an ultrathin (<50 nm) polycrystalline ice deposit

By using proton-ordered and disordered Ic and Ih ice models, Buch and Devlin (33) made use of four oscillating dipoles tetrahedrally arranged around a central O atom as the basis to calculate the OH stretching band. They attributed the central peak of the OH stretching band at 3220 cm^{-1} to the zero wave-vector modes of two transversal (TO) branches and a longitudinal (LO) branch (which corresponds to two dipoles moving “in” with the other two dipoles moving “out” in a way that correlates with the asymmetric stretching character of the ν_3 molecular mode of an isolated water molecule). The asymmetric ν_3 character of the OH central peak is in agreement with the spectral assignment made by Whalley (34). The shoulder located at the lower-frequency side of the central peak appears to originate from the transversal modes strongly perturbed by intramolecular interactions and was therefore attributed to the in-phase ν_1 TO branch by Buch and Devlin (33), again in accord with Whalley’s earlier assignment (34). The state with the lowest OH stretch frequency corresponds to the globally in-phase ν_1 vibration, which dominates in the Raman spectra obtained with parallel polarization (38). In the higher-frequency region of the OH stretching band, an intermediate branch (i.e., one that exhibits no systematic variation in the angle between the dipole moment of the lattice and the wave-vector) and nonzero wave-vector modes of the aforementioned longitudinal branch were found (33). Originated from the higher-frequency out-of-phase ν_1 vibration of the four dipoles surrounding the O atom, the intermediate branch was characterized by a small dipole moment near the center of the Brillouin zone, in marked contrast to the longitudinal modes (with origin from the ν_3 molecular vibration), which carry a significant dipole moment over the entire Brillouin zone (33).

Buch and Devlin (33) further demonstrated that the OH stretch absorption band can be strongly affected by the shape of the ice medium and by the polarization of the electric field. In particular, in the case of an ice slab, the modes of the higher-frequency intermediate and longitudinal branches are stimulated with surface-perpendicular polarization, while the lower-frequency transversal modes of the ν_1 branch are preferentially excited with surface-parallel polarization. The dependence of the absorption spectra on the shape is caused by the long-range dipole-dipole interaction, which was found to include a shape-dependent component associated with the surface polarization charge (39). The oscillating surface charge creates an electric field inside the sample that changes the energy gap between the ground and excited vibrational levels (39), and consequently the corresponding vibrational frequencies become shape-dependent. However, the shape-dependent effect predicted by the model was found to be considerably stronger than that observed experimentally (33). This discrepancy was attributed to a limitation on the spatial extent of the vibrational excited states imposed by the imperfections in the pc-ice medium.

The Buch–Devlin simulation of IR absorption by an ice slab for the surface-perpendicular polarization (33) could be directly compared with the experimental RA spectra of ultrathin ice films on a metal surface at grazing-angle illumination with π -polarized or nonpolarized light. Upon reflection on a highly conductive metal, the σ -polarized component of the incident electric field is almost completely eliminated near its surface and only the π -polarized component of the electric field remains, which provides the physical justification for comparing the experimental RA spectra with the simulated spectrum for excitation of an ice slab by just the (surface-perpendicular) π polarization. In particular, the Buch–Devlin model (33) predicts that the absorption spectra of the ice slab for the surface-perpendicular polarization are primarily originated from excitation of the intermediate and ν_3 LO branches, of which the former is of a higher frequency. Figure 3 compares our experimental RA spectra of the OH stretching band obtained for ultrathin pc-ice deposits (with an estimated thickness below 50 nm) with the corresponding Fresnel spectra and with the Berreman and transmission profiles (40) (arbitrarily normalized to the band maxima of the respective experimental spectra). The Berreman profile corresponds to the energy loss function defined as $\text{Im}(-\epsilon^{-1}) = \epsilon''/(\epsilon'^2 + \epsilon''^2)$, where the dielectric function $\epsilon = \epsilon' - i\epsilon''$ (with its real ϵ' and imaginary ϵ'' parts), while the transmission profile is given by $\text{Im}(\epsilon)$ (i.e., ϵ''). The Fresnel spectra and both of these profiles are generated based on the spectral data reported by Toon et al. (28). Evidently, the spectra for pc-ice deposited at 160 K and 1×10^{-6} torr (1 torr = 133.322 4 Pa) for 30 and 45 s (curves A and B, Fig. 3a) are in good accord in shape with the Buch–Devlin spectrum for the ice slab (see Fig. 3c in ref. 33), supporting the assignment of the higher-frequency shoulder at 3365 cm^{-1} to the intermediate branch and of the 3280-cm^{-1} feature to the ν_3 LO band. The band maximum for the 3280 cm^{-1} peak is also found to be in good agreement with that of the ν_3 LO band (3299 cm^{-1}) predicted by Whalley (34). Furthermore, the 45 s spectrum (curve B, Fig. 3a) closely follows the energy loss function as represented by the Berreman profile (curve E, Fig. 3a), which again indicates that the blue shift of the central OH stretch peak with respect to the transmission profile (curve D, Fig. 3a) is due to stimulation of the longitudinal modes of the ν_3 branch. The apparent enhancement of the higher-frequency part of the OH stretch with the corresponding weakening of the lower-frequency part could be associated with the blue shift of the most intense ν_3 branch alone and not to the actual changes in their own respective intensities. As expected for thicker deposits, the 115 s RA spectrum shown in Fig. 3b (curve F) evidently begins to deviate from the Berreman profile (curve H, Fig. 3b) and converge to the Fresnel spectrum (curve G, Fig. 3b), indicating the onset of the formation of a stratified ice film with smooth interfaces. The continual blue shift of the OH stretch and the apparent changes in the relative intensities of the band components (band shape deformation) with increasing thickness are likely caused by optical effects in the film on a metal substrate (41). Accordingly, at the initial stage of pc-ice film formation the ice deposit exists in the form of crystallites, which causes the experimental spectra to deviate from the Fresnel model. This is illustrated by the differences between the 30 and 45 s

Fig. 3. Comparison of the OH stretching band of the experimental FT-IR–RA spectra of early-stage polycrystalline (pc) ice deposits obtained by vapour deposition at 160 K and 1×10^{-6} torr (1 torr = 133.322 4 Pa) for 30 s (A), 45 s (B), and 115 s (F) with the Fresnel spectra of 20 nm (C) and 53 nm (G) thick pc-ice films and the Berreman (E, H) and transmission profiles (D), all arbitrarily normalized.

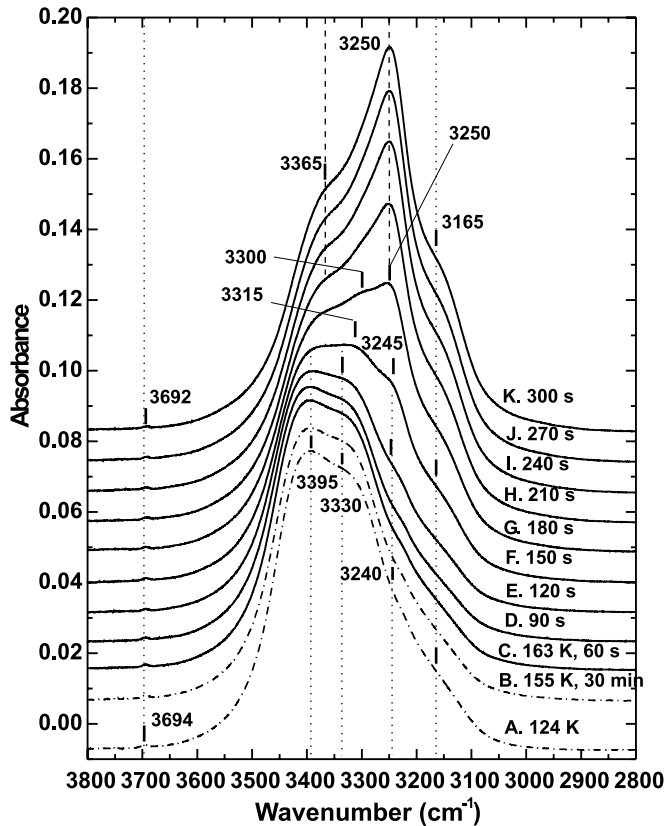


spectra (both with a common shape, curves A and B in Fig. 3a) and the corresponding Fresnel spectrum. In this case, the frequency position of a band associated with the ν_3 LO modes becomes dependent upon the particle shapes of the crystallites (31, 32, 38, 39).

Temporal evolution of the OH (OD) stretch manifold during crystallization of an ultrathin, noncrystalline ice deposit

Because nc ice is considered metastable with respect to the crystalline ice form, annealing of an nc-ice deposit could promote crystallization to occur at a detectable rate above an appropriate temperature. Indeed, rapid changes in the OH stretch region are found at 153–163 K in the present work, in good accord with the earlier observations made by using different techniques (16, 17, 23). In particular, Fig. 4 shows the temporal evolution of the OH stretching band at 155 K for 30 min and at 163 K for 6 min for an nc-ice film deposited at 124 K and 1×10^{-6} torr (1 torr = 133.322 4 Pa) for 240 s. In Fig. 5, we compare selected experimental profiles in Fig. 4 with the appropriate calculated spectra. While no significant temporal spectral changes are found at 155 K

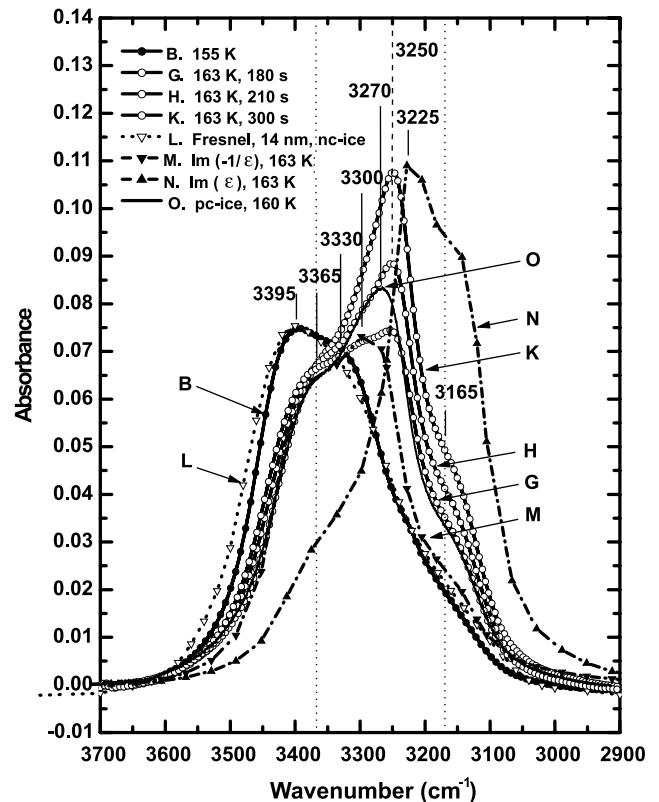
Fig. 4. Evolution of the OH stretching band of the experimental FT-IR-RA spectra for an early-stage, noncrystalline ice deposit obtained by vapour deposition at 124 K and 1×10^{-6} torr (1 torr = 133.322 4 Pa) for 240 s (A), followed by annealing to 155 K for 30 min (B), and to 163 K for 60 s (C), 90 s (D), 120 s (E), 150 s (F), 180 s (G), 210 s (H), 240 s (I), 270 s (J), and 300 s (K).



(curve B, Fig. 4) relative to the as-deposited nc-ice spectrum at 124 K (curve A, Fig. 4), rapid dramatic changes in the shape of the OH stretching band are observed at 163 K (curves C–K, Fig. 4). By analogy with the assignment for pc ice, the weak peak at 3694 cm^{-1} can be attributed to the OH dangling bonds, while the features at 3395 , 3330 , and 3165 cm^{-1} likely correspond to the out-of-phase ν_1 intermediate modes, the ν_3 LO branch, and the in-phase ν_1 branch, respectively. As shown in Fig. 5, the OH stretch profiles for the nc-ice film as-deposited at 124 K and upon annealing to 155 K (curve B, Fig. 5) are well approximated by the Fresnel spectrum for a 14 nm thick nc-ice film (curve L, Fig. 5), indicating the preservation of the smooth stratified film even upon annealing at 155 K for 30 min. On the other hand, discernible spectral changes near 3245 cm^{-1} are found upon annealing at 163 K for just 2 min (curves C–E, Fig. 4). This feature develops into a strong, well-defined peak at 3250 cm^{-1} upon further annealing at the same temperature for 3 more min (curves F–K, Fig. 4). In contrast, the dangling-bond feature at 3694 cm^{-1} remains essentially unchanged except for the minor red shift during this anneal.

Figure 5 also compares selected spectra obtained during the 163 K anneal with the RA spectrum of the 30 s pc-ice film deposited at 160 K discussed earlier in Fig. 3, and with

Fig. 5. Comparison of the OH stretching band of the experimental FT-IR-RA spectra of an early-stage, noncrystalline (nc) ice deposit obtained by vapour deposition at 124 K and 1×10^{-6} torr (1 torr = 133.322 4 Pa) for 240 s followed by annealing to 155 K for 30 min (B) and to 163 K for 180 s (G), 210 s (H), and 300 s (K) with that of a polycrystalline (pc) ice deposit obtained by vapour deposition at 160 K and 1×10^{-6} torr (1 torr = 133.322 4 Pa) for 30 s (O), and with the Fresnel spectrum of a 14 nm thick nc-ice film (L) and the Berreman (M) and transmission profiles for the pc ice (N), all arbitrarily normalized.

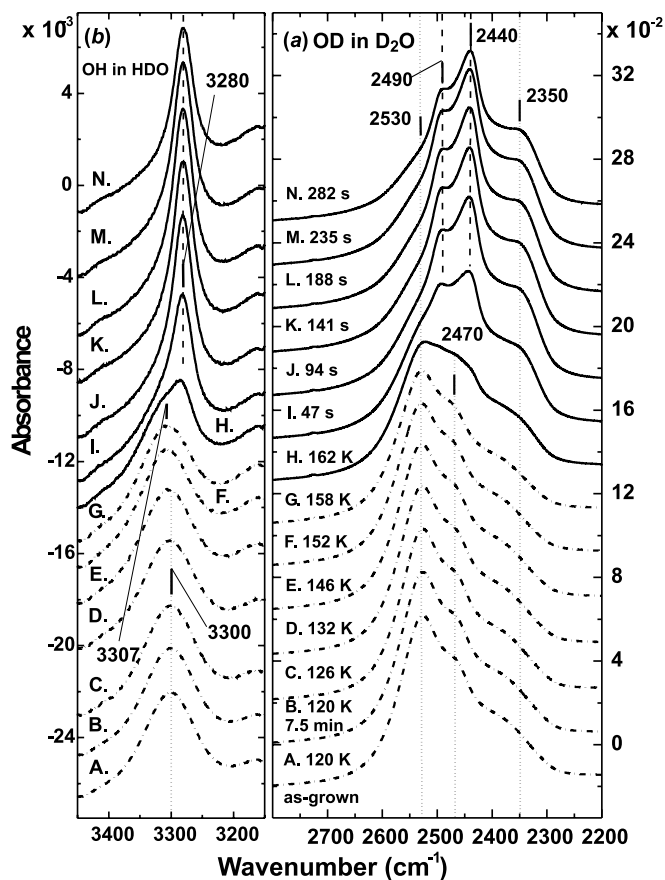


the Berreman and transmission profiles for pc-ice films. Evidently, the major differences between the OH stretch profiles of the annealed nc-ice film (curves G, H, and K, Fig. 5) and that of the as-grown 30 s pc-ice film (curve O, Fig. 5) are the location and relative intensity of the ν_3 LO manifold (at 3250 vs. 3270 cm^{-1}). According to the theoretical study by Wojcik et al. (42), the emergence of a prominent ν_3 LO band during annealing in the present work can be used as evidence of a rapid increase in the density of excited vibrational states in this narrow frequency region, which in turn indicates the onset of a crystallization process. The intensity increase of the overall OH stretching band during the anneal (curves G, H, and K, Fig. 5) is also consistent with the general chemical principle that crystallization leads to strengthening of the hydrogen bonds in the ice medium (43). Furthermore, the peak maximum of the observed ν_3 band (3250 cm^{-1}) is found to be in between those of the Berreman profile (3300 cm^{-1} , curve M, Fig. 5) and the transmission profile (3225 cm^{-1} , curve N, Fig. 5). (It should be noted that the Berreman profile and the transmission profile are arbitrarily normalized to the experimental spectra shown as curve G and curve K, respectively.) The intermediate peak

location is due to the presence of surface modes in the crystallites, as discussed by Englman and Ruppin (31) and Martin (32). Moreover, the formation and growth of the crystallites introduce tension into the film and could lead to cracking in a sufficiently thin film.

Figure 6 shows the temporal evolution of the OH and OD stretching modes of deuterated nc ice as deposited at 120 K and 1.5×10^{-6} torr (1 torr = 133.322 4 Pa) for 9 min and during annealing to 162 K. Evidently, no discernible change is observed in the OD stretching mode upon annealing from 120 to 162 K (curves A–H, Fig. 6a). Furthermore, the temporal evolution in the OD stretch features at 162 K for nearly 5 min (curves H–N, Fig. 6a) is found to be remarkably similar to that of the OH stretch observed earlier in the undeuterated nc-ice sample (Figs. 4 and 5), which again indicates the onset of rapid crystallization at this temperature. (Figure 6a also shows only minor changes in the dangling-bond signal of the OD surface groups at 2727 cm^{-1} during crystallization). Moreover, the uncoupled OH stretching mode of HOD in the deuterated ice sample exhibits a red shift from 3300 cm^{-1} at 120 K (curve A, Fig. 6b) to 3280 cm^{-1} at 162 K (curve N, Fig. 6b) with concomitant narrowing of the peak, which is also consistent with the crystallization process. The changes in this vibrational mode are in excellent agreement with the transmission spectra for thick amorphous and polycrystalline ice samples obtained by Bergren et al. (44). Between 120 K (curve A, Fig. 6b) and the crystallization onset at 162 K (curve H, Fig. 6b), there is a small but discernible blue shift of 7 cm^{-1} accompanied with peak broadening in this structure-sensitive mode, which could be argued as spectral evidence for further disordering of this nc-ice deposit immediately before crystallization. This spectral change might also be associated with an endothermic peak in the calorimetric upscan of an nc-ice medium often appearing just before the crystallization onset, which has been attributed to a glass-to-liquid transition in the earlier studies (16, 17) because frequency shifts for the structure-sensitive modes (including, e.g., the aforementioned modes) are expected in the case of a supercooled liquid state. In particular, Jenniskens et al. (45) used this approach to interpret their FT-IR–RAS data for the transition of nc ice to pc ice. Smith and Kay (19) and Smith et al. (20) also attributed the significant enhancement in the self-diffusivity of nc ice over this temperature range to a glass-to-liquid transition. However, the observed blue shift for this nc-ice feature is also in remarkably good agreement with the blue shift of the corresponding feature for pc-ice solids upon annealing (from 3275.2 cm^{-1} at 120 K to 3280.5 cm^{-1} at 150 K) observed by Sivakumar et al. (46) using Raman spectroscopy. Indeed, we also observed a corresponding red shift in the OH stretch feature in the crystallized ice (curve N, Fig. 6b) upon recooling from 162 to 120 K (not shown). The blue shift in the isolated OH stretch observed for nc ice upon annealing in the present work is therefore most likely just the natural consequence of thermal expansion of the ice medium. We favour the latter, simpler explanation over the former explanation invoking the glass-to-liquid transition because such an equilibrium thermodynamic effect is expected to occur regardless of the existence of the glass-to-liquid transition. Together with the early spectroscopic studies on ice crystallization by Hardin and Harvey (36) and

Fig. 6. Evolution of (a) the OD stretching band (for D_2O) and (b) the OH stretching band (for HDO) of the experimental FT-IR–RA spectra for an early-stage noncrystalline ice deposit obtained by vapour deposition at 120 K and 1.5×10^{-6} torr (1 torr = 133.322 4 Pa) for 9 min (A), followed by annealing to 120 K for 7.5 min (B) and to 132 K (C), 146 K (E), 152 K (F), 158 K (G), and 162 K (H) for 47 s (I), 94 s (J), 141 s (K), 188 s (L), 235 s (M), and 282 s (N).



Hagen et al. (47), the present data therefore provides no conclusive spectroscopic evidence for the existence of a distinct glass-to-liquid transition in nc ice in the 120–163 K range. Although any difference in the rates of relaxation processes is expected to manifest in the shape and width of the OH stretch band, we cannot rule out the possibility that the local structures of the water glass and supercooled liquid states happen to be almost identical, in which case the intermolecular interactions in both media are so close to each other that no spectral differences in the OH (OD) stretching region could be resolved. In a separate experiment, we also obtained FT-IR–RA spectra for an organic guest species, acetone or acetaldehyde, codeposited with water to form a noncrystalline guest–ice matrix at 130 K (48). The temporal evolution of the spectral features of the embedded guest species upon annealing followed by crystallization of the ice at 165 K shows only steady escape of the guest species from the matrix. While spectral differences between the adsorption (absorption) states of the guest species in the nc- and pc-ice samples were clearly resolved, no signature of the intermediate states in the guest-supercooled liquid water matrix in the 130–165 K temperature region could be observed

(48). Similar spectral observations of a steady escape and the absence of any frequency shift for dimethyl ether in a dimethyl ether – water matrix at 130–160 K have also been reported recently by Schriver-Mazzuoli et al. (49), although the spectral changes for dimethyl ether have been found at 120–130 K and attributed to clathrate–hydrate formation (49). These results further support our above observation of direct transition from nc ice to pc ice (i.e., without an intermediate glass-to-liquid transition). Furthermore, the results on crystallization kinetics of thin compact nc ice films by Dohnalek et al. (22) are also consistent with the direct solid-to-solid phase transformation.

It should be noted that for thicker ice deposits, for example those above 100 nm thick shown in Figs. 1 and 2, the temporal evolution of the main peak in the OH or OD stretch manifold upon annealing followed by crystallization is found to be less pronounced, likely due to the optical effects of the film–metal medium as discussed earlier by La Spisa et al. (50).

Concerning the state of surfaces at nc-ice and pc-ice films investigated in the present and early studies (25), it should be noted that the amount of OH dangling bonds as estimated by the intensity of the corresponding spectral feature at 3694 cm^{-1} (Fig. 4) on the as-grown thin (and compact) nc-ice films is similar to that on the pc-ice films prepared by crystallization of nc-ice films or by direct deposition. However, our FT-IR–RAS data on acetone adsorption (48, 51) appear to indicate a dynamical difference in the surface states of the adsorbate on nc- and pc-ice films. This difference is clearly related not only to the “snap-shot” structure of the surface but also to the stability and dynamics of the surface and near-surface regions of nc- and pc-ice films as discussed by Buch et al. (52).

Concluding remarks

The temporal evolution of the OH (and OD) stretch manifold(s) in the (deuterated) nc-ice deposits upon annealing followed by crystallization has been investigated by using FT-IR–RAS at grazing-angle incidence. We provide a microscopic interpretation of the spectral data using the theoretical results of Buch and Devlin (33) and Whalley’s assignment (34). For the ultrathin nc-ice deposits, crystallization near 160 K has been demonstrated for the first time to be marked spectroscopically by an abrupt enhancement along with a concomitant red shift in the longitudinal branch of the ν_3 OH (OD) stretching mode at 3250 (2440) cm^{-1} . These observations are consistent with strengthening of the hydrogen bonds in the molecular water network and with increased ordering of an ice medium during crystallization. Furthermore, the spectral dynamics of the OH and OD stretch manifolds and of the isolated OH stretching mode in a deuterated ice matrix near 160 K observed in the present work indicate that rapid crystallization proceeds directly from a noncrystalline to a crystalline state, i.e., without any long-lived intermediate state that involves a hydrogen-bonded network structurally different from that of nc ice at a lower temperature (120 K). While the present interpretation of the OH spectral dynamics does not favour the existence of a glass-to-liquid transition during crystallization, we cannot rule out the existence of a supercooled-liquid state that happens to have a

nearly identical local structure to glass. Further studies possibly involving non-spectroscopic data would be of great interest to resolve this intricate fundamental issue about ice.

Acknowledgement

This work was supported by the Natural Sciences and Engineering Research Council of Canada (NSERC).

References

1. P.V. Hobbs. Ice physics. Clarendon Press, Oxford. 1974.
2. O. Mishima and H.E. Stanley. Nature (London), **396**, 329 (1998).
3. O. Mishima. J. Chem. Phys. **100**, 5910 (1994).
4. J.L. Finney, D.T. Bowron, A.K. Soper, T. Loerting, E. Mayer, and A. Hallbrucker. Phys. Rev. Lett. **89**, 205 503 (2002).
5. J.L. Finney, A. Hallbrucker, I. Kohl, A.K. Soper, and D.T. Bowron. Phys. Rev. Lett. **88**, 225 503 (2002).
6. A.I. Kolesnikov, J. Li, S.F. Parker, R.S. Eccleston, and C.-K. Loong. Phys. Rev. B, **59**, 3569 (1999).
7. V.P. Shpakov, P.M. Rodger, J.S. Tse, D.D. Klug, and V.R. Belosludov. Phys. Rev. Lett. **88**, 155 502 (2002).
8. V.P. Voloshin, E.A. Zhelegovskaya, G.G. Malenkov, and Yu.I. Naberukhin. J. Struct. Chem. **42**, 794 (2001).
9. H. Tanaka. J. Chem. Phys. **105**, 5099 (1996).
10. J.P. Devlin and V. Buch. J. Phys. Chem. **99**, 16 534 (1995).
11. K.P. Stevenson, G.A. Kimmel, Z. Dohlanek, R.S. Smith, and B.D. Kay. Science, **28**, 1505 (1999).
12. Z. Dohlanek, G.A. Kimmel, P. Ayotte, R.S. Smith, and B.D. Kay. J. Chem. Phys. **118**, 364 (2003).
13. E. Mayer and R. Pletzer. Nature (London), **319**, 298 (1986).
14. D. Laufer, E. Kochavi, and A. Bar-Nun. Phys. Rev. B, **36**, 9219 (1987).
15. M.S. Westley, G.A. Baratta, and R.A. Baragiola. J. Chem. Phys. **108**, 3321 (1998).
16. I. Kohl, E. Mayer, and A. Hallbrucker. Phys. Chem. Chem. Phys. **2**, 1579 (2000).
17. A. Hallbrucker, E. Mayer, and G.P. Johari. J. Phys. Chem. **93**, 4986 (1989).
18. M.A. Zondlo, T.B. Onasch, M.S. Warshawsky, M.A. Tolbert, G. Mallick, P. Arentz, and M.S. Robinson. J. Phys. Chem. B, **101**, 10 887 (1997).
19. R.S. Smith and B.D. Kay. Nature (London), **398**, 788 (1999).
20. R.S. Smith, Z. Dohnalek, G.A. Kimmel, K.P. Stevenson, and B.D. Kay. ACS Symposium Series 820. American Chemical Society, Washington, D.C. 2002. p. 198.
21. Z. Dohnalek, R.L. Ciolli, G.A. Kimmel, K.P. Stevenson, R.S. Smith, and B.D. Kay. J. Chem. Phys. **110**, 5489 (1999).
22. Z. Dohnalek, G.A. Kimmel, R.L. Ciolli, K.P. Stevenson, R.S. Smith, and B.D. Kay. J. Chem. Phys. **112**, 5932 (2000).
23. D.R. MacFarlane and C.A. Angell. J. Phys. Chem. **88**, 759 (1984).
24. V. Velikov, S. Borick, and C.A. Angell. Science, **294**, 2335 (2001).
25. S. Mitlin and K.T. Leung. J. Phys. Chem. B, **106**, 6234 (2002).
26. R.G. Greenler. J. Chem. Phys. **44**, 310 (1966).
27. J.D.E. McIntyre and D.E. Aspnes. Surf. Sci. **24**, 417 (1971).
28. O.B. Toon, M.A. Tolbert, B.G. Koehler, and A.M. Middlebrook. J. Geophys. Res. **99**(D12), 631 (1994).
29. A. Leger, S. Gauthier, D. Deforneau, and D. Rouan. Astron. Astrophys. **117**, 164 (1983).
30. B. Mate, A. Medialdea, M.A. Moreno, R. Escibano, and V.J. Herrero. J. Phys. Chem. B, **107**, 11 098 (2003).

31. R. Englman and R. Ruppin. *J. Phys. C. (Proc. Phys. Soc.)* **1**, 614 (1968).
32. T.P. Martin. *Phys. Rev.* **177**, 1349 (1969).
33. V. Buch and J.P. Devlin. *J. Chem. Phys.* **110**, 3437 (1999).
34. E. Whalley. *Can. J. Chem.* **55**, 3429 (1977).
35. C. Haas, D.F. Hornig. *J. Chem. Phys.* **32**, 1763 (1960).
36. A.H. Hardin and K.B. Harvey. *Spectrochim. Acta*, **29A**, 1139 (1973).
37. J.E. Bertie and E. Whalley. *J. Chem. Phys.* **40**, 1637 (1964).
38. J.P. Devlin. *J. Chem. Phys.* **90**, 1322 (1989).
39. D. Fox and R. Hexter. *J. Chem. Phys.* **41**, 1125 (1964).
40. D.W. Berreman. *Phys. Rev.* **130**, 2193 (1963).
41. R.G. Tobin. *Phys. Rev.* **45**, 12 100 (1992).
42. M.J. Wojcik, V. Buch, and J.P. Devlin. *J. Chem. Phys.* **99**, 2332 (1993).
43. A.V. Iogansen. *Spectrochim. Acta*, **A55**, 1585 (1999).
44. M.S. Bergren, D. Schuh, M.G. Sceats, and S.A. Rice. *J. Chem. Phys.* **69**, 3477 (1978).
45. P. Jenniskens, S.F. Banham, D.F. Blake, and M.R.S. McCoustra. *J. Chem. Phys.* **107**, 1232 (1997).
46. T.C. Sivakumar, S.A. Rice, and M.G. Sceats. *J. Chem. Phys.* **69**, 3468 (1978).
47. W. Hagen, A.G.G.M. Tielens, and J.M. Greenberg. *Chem. Phys.* **56**, 367 (1981).
48. S. Mitlin, and K.T. Leung. (2004) to be published.
49. L. Schriver-Mazzuoli, J.M. Coanga, A. Schriver, and P. Ehrenfreund. *Vib. Spec.* **30**, 245 (2002).
50. S. La Spisa, M. Waldheim, J. Lintemoot, T. Thomas, J. Naff, and M. Robinson. *J. Geophys. Res.* **106**(E12), 33 351 (2001).
51. S. Mitlin and T. Leung. *Surf. Sci.* **505**, L227 (2002).
52. V. Buch, L. Delzeit, C. Blackledge, and J.P. Devlin. *J. Phys. Chem.* **100**, 3732 (1996).